LBL-29222

Lawrence Berkeley Laboratory
UNIVERSITY OF CALIFORNIA

EARTH SCIENCES DIVISION

Presented at the 65th Annual Technical Conference and Exhibition, New Orleans, LA, September 23–26, 1990, and to be published in the Proceedings

A Dual-Gas Tracer Technique for Determining Trapped Gas Saturation during Steady Foam Flow in Porous Media

J.V. Gillis and C.J. Radke

June 1990

Prepared for the U.S. Department of Energy under Contract Number DE-AC03-76SF00098

DISCLAIMER

LBL-29222

A Dual-Gas Tracer Technique for Determining Trapped Gas Saturation during Steady Foam Flow in Porous Media

J. V. Gillis and C. J. Radke

Earth Sciences Division
Lawrence Berkeley Laboratory
University of California
Berkeley, California 94720

and

Chemical Engineering Department
University of California

June 1990

This work was supported by the U.S. Department of Energy under Contract No. DE-AC03-76SF00098.

ABSTRACT

Foam is a possible mobility control agent for effective oil displacement from reservoirs. Thus, it is important to understand the mechanisms by which foam flows in porous media. Micromodel studies and prior gas-phase tracer experiments show that a significant fraction of the gas in a foam exists as trapped bubbles which, therefore, have a major impact on the flow resistance. Unfortunately, in the tracer experiments performed to date, partitioning of the tracer into the trapped gas has not been accounted for. Currently, only qualitative information is available on the actual amounts of trapped gas.

To overcome these limitations and obtain quantitative measurements of trapped gas saturations, we have developed a unique experimental apparatus employing dual gas tracers. During steady foam flow in a porous medium, dilute sulfur hexafluoride (SF_6) and methane (CH_4) tracers in a nitrogen carrier are injected, and the effluent concentration is monitored by gas chromatography. The measured tracer histories are fit to a simple mass transfer model which describes any partitioning between the mobil and trapped

foam phases. Tracer effluent concentrations predicted by the model are strongly influenced by the solubility of each tracer in the liquid phase. This behavior is observed in the experimental histories as well. Hence, multiple gas tracers provide a discriminating assessment of trapped gas saturation during foam flow through porous media.

New trapped gas saturations are reported for an aqueous C_{14-16} α-olefin sulfonate foamer solution and nitrogen flowing through a 2.3-μm^2 fired Berea sandstone at 10^5 Pa (1 atm) back pressure and at room temperature. Total superficial velocities range from 0.4 to 4 m/day while inlet gas fractional flows are varied from 0.8 to 1.0. We find large fractions of trapped gas between 80 and almost 100% depending on the particular flow conditions. The importance of trapped gas to understanding foam-flow behavior is again confirmed.

INTRODUCTION

Foam has been shown to exhibit high apparent viscosities in porous media [1-3]. This leads to a vast improvement in the mobility ratio of, for example, a steam or CO_2 flood. Both gravity override and channeling through high permeability zones are reduced when these fluids flow in the form of a foam. In addition, foam is relatively easy to apply. Its major component is gas, and the surfactants which stabilize the foam can be used in amounts on the order of 1 weight % of the liquid phase.

There are numerous, important pore-level phenomena involved in foam flow in porous media [4,5]. One of the most important of these, and the subject of this paper, is trapped gas saturation. When foam transports through a porous medium not all of the gas in the foam actually flows. Several investigators have reported visual observations of appreciable bubble trapping in

transparent micromodels and beadpacks [4-10]. Figure 1, sketched from the etched-glass micromodel observations of Chambers [5], shows two origins of foam bubble trapping. In this figure shaded foam bubbles are trapped in the upper and lower channels which exhibit small pore throats. Flowing foam, shown clear, transports as bubble trains around the trapped clusters and through the intervening constricted pore characterized by large pore throats. Dark arrows locate the particular throats causing blockage. Trapping in the upper pore channel is due to a lamella residing just at the exit of the right most small pore throat, which terminates sharply into a downstream pore body. Lamellae in such configurations require large pressure drops to be mobilized [6,11]. The trapped bubble cluster in the bottom most pore of Fig. 1 abuts against a wetting liquid lens (or against continuous liquid). Here mobilization demands a pressure drop sufficient to overcome the large capillary entrance pressure of the throat [4,5,11].

Trapped foam is important because it can block large fractions of the cross sectional area available to gas flow. Equivalently, the relative permeability to foam [2,3] is drastically reduced. Thus, quantifying the amount of trapped gas is critical to predicting foam flow resistance in porous media. Throughout the following discussion, trapped gas saturation is the ratio of trapped gas volume to total pore volume, whereas the trapped gas fraction is defined as the ratio of trapped gas volume to total gas volume.

Fried was the first to theorize and confirm experimentally that foam increases the trapped gas saturation in a porous medium [12]. After foam flooding a core and then displacing the foam with distilled water, he found the gas saturation to be 27%. (We note parenthetically that with continued injection of surfactant-free liquid the foam will eventually collapse and

alter the gas saturation. However, this may require a large amount flushing [13]). A similar experiment without foam gave a gas fraction of only 4%. Unfortunately, Fried's technique is valid only for a unity fractional flow of water and cannot give a value for the trapped gas fraction during foam flow. However, it remains useful as the first measurement of trapped gas fraction for a foam system in porous media.

Bernard, Holm, and Jacobs later used a method similar to Fried's to measure trapped gas saturations for different surfactant concentrations and different porous media [14]. They found that, in general, the trapped gas saturation increases with increasing surfactant concentration and with increasing permeability of the medium. They also showed that the amount of trapped gas is reduced in the presence of oil. The reported values of trapped gas saturation are in the range of 10-70%. As in Fried's experiments, these reported values are for a waterflood following a foam flood. They do not necessarily represent the trapped gas saturation in steady foam flow.

A practical way to measure trapped gas saturation during a foam flood is to trace the gas phase. Holm made use of both gas and liquid-phase tracers to study dispersion in the presence of foam in 5.0-μm^2 sandpacks [15]. He confirmed in several different experiments that the presence of foam increased the degree of gas-phase dispersion relative to that with no foam present. Unfortunately, he made no attempt to relate the measured tracer concentration histories to the trapped gas saturation.

Nahid was, apparently, the first to report values of trapped gas saturation measured during foam flow [16]. He studied foam flowing in a fired Berea sandstone at connate water saturation. Helium was the bulk gas and a mixture of 80% helium and 20% methane served as the tracer gas. A step change

in concentration was injected into the core, and methane concentrations were measured at the core outlet by gas chromatography. Nahid found that up to 32% of the gas was trapped for a 1% by weight Triton X-100 nonionic surfactant solution. Lower surfactant concentrations gave smaller trapped gas fractions. In order to extract quantitative trapped foam fractions from the tracer histories, Nahid assumed that partitioning of the tracer through the liquid and into the trapped gas was negligible.

Friedmann, Chen, and Gauglitz recently presented gas-phase tracer experiments for steady foam flow in a Berea core at 150°C [17]. The bulk gas was N_2 and the tracer was krypton. For a range of gas frontal advance rates of 25 to 130 m/day, they reported a mean value of 0.15 for the flowing gas fraction. These authors also observed large amounts of tailing of the tracer caused by mass transfer into the trapped gas phase. They made no attempt to correct for this effect. Rather, an ad hoc technique was adopted in which the number of pore volumes of gas injected for a 10% normalized tracer concentration was ascertained for similar systems with and without foam. The ratio of these two pore volumes was taken to be the flowing gas fraction.

The experimental, gas-tracer histories of Holm, Nahid, and Friedmann, Chen, and Gauglitz all suggest significant transfer into the trapped foam fraction which clouds interpretation. The purpose of this work is to obtain more quantitative estimates of foam trapping by accounting for such mass transfer effects. This goal is accomplished first by utilizing two simultaneous, noninteracting gas tracers, each with different but low brine solubilities, and second by modeling the mass transfer resistances that abate partitioning into the trapped foam bubbles.

In the proceeding section our proposed mass transfer model and its physical underpinnings are highlighted. The unique dual-gas tracer experiments, using methane and sulfur hexafluoride in nitrogen, are then described. New results follow for steady foam flow in a 2.3-μm^2 Berea sandstone with a 1 weight % α-olefin surfactant over gas fractional flows varying from 80 to 99% and for total superficial velocities ranging from 0.4 to 4 m/day. We find large trapped foam fractions up to 99% depending on the flow conditions.

MASS TRANSFER MODELING

Construction of a macroscopic tracer transport model for flowing foam in porous media requires some understanding of how foam is distributed topologically in the pore space. Our picture of foam microstructure is portrayed in Fig. 2 [2-5]. In this schematic, cross-hatched circles represent sand grains and dotted space indicates wetting liquid. For illustration purposes only, pore channels are arranged with the largest size at the top. As in Fig. 1, flowing foam bubbles are clear, whereas trapped bubbles are shaded.

Because of capillary forces, wetting liquid occupies the smallest pores and transports in continuum multiphase flow. These strong, liquid-wetting forces compel the foam to be the nonwetting fluid. Foam trapping occurs in the intermediate size pores. Both mechanisms of trapping in Fig. 1 demand larger mobilization pressure drops in smaller pore throats. Hence, foam bubbles are trapped by pore throats whose sizes lie above those occupied by the liquid phase.

Foam transports as bubbles trains in the very largest channels. Here its flow resistance is lower, relative to that of the smaller pore-size paths. At

steady state it is possible, but unlikely, that some of the very largest channels contain free gas.

Figure 2 is highly schematic and does not suggest that at the pore level foam bubbles are organized vertically above the more dense wetting liquid. (This may occur, of course, on a reservoir scale.) Rather, the liquid-occupied, trapped-foam, and flowing-foam channels are highly convoluted and interwoven. Nevertheless, Fig. 2 provides insight into why gas-tracer mass transfer effects might be important.

As gas tracer convects in the bubble trains, some of it dissolves into the surrounding liquid and convectively diffuses into the fringes of the nearest stagnant bubbles. Because gas-phase diffusion coefficients are relatively large, the tracer soon reaches the opposite side of these trapped bubbles. It then dissolves into the thin lamellae and rapidly enters adjacent trapped bubbles. For example, with a liquid-phase tracer diffusion coefficient of $D_L = 10^{-5}$ cm^2/s and a lamella thickness of 100 nm, the time to penetrate through a foam lamella is $O(10^{-5})$ s. In this manner, many stagnant foam bubbles can be contacted by the tracer. A very simple macroscopic model is presented below to describe this partitioning phenomenon.

Picture trapped gas bubbles separated laterally from the flowing gas by water sheaths, either in the pendular regime or as water-occupied pores. These cushioning water layers provide the main resistance to mass transfer into the trapped gas. The average thickness of the sheaths is defined as δ. Let S_T, S_F, and S_L represent the steady saturations of the trapped gas, mobile gas, and intervening liquid sheaths in a one-dimensional core of porosity ϕ and length L. If the axial dispersion coefficient, D, varies linearly with

gas velocity and if the gas is ideal, then tracer mass conservation in the mobile gas reads in nondimensional form:

$$(1-\alpha)\frac{\partial C_F}{\partial t} + \frac{\partial\left[C_F/P\right]}{\partial x} = \frac{1}{Pe}\frac{\partial}{\partial x}\left[P\frac{\partial\left[C_F/P\right]}{\partial x}\right] + Da\left.\frac{\partial C_L}{\partial y}\right|_{y=0}, \qquad (1)$$

where $t \equiv U_{go}t^*/[\phi(S_F + S_T)L]$ is a nondimensional time or pore volumes of gas injected for an inlet superficial gas velocity of U_{go}, $x \equiv x^*/L$ is the reduced axial column length, and $y \equiv y^*/\delta$ is a reduced lateral distance. C_F and C_L are the flowing-gas and liquid-phase tracer concentrations nondimensionalized by the exit tracer concentration after infinite time $c_{FL}(\infty)$. P denotes the ratio of local to inlet gas pressures P_g/P_{go}. It reflects gas compressibility.

Parameters in Eqn. (1) include

$$\alpha \equiv S_T/(S_F + S_T)\ , \qquad (2a)$$

$$Pe \equiv U_{go}L/D\ , \qquad (2b)$$

and

$$Da \equiv \phi\ S_L\ D_L/U_{go}\delta^2\ . \qquad (2c)$$

α is the fraction of trapped gas. It is the quantity that we are primarily interested in. The parameter Pe is a column Peclet number gauging tracer convection versus axial dispersion. Finally, Da is a mass transfer Damköhler number representing the relative roles of tracer convective-diffusion in the water sheaths and tracer convection in the mobile gas. Equation (1) does not explicitly recognize the rapid making and breaking of lamellae in the mobile gas regime [2-5,18,19]. Such processes should not abrogate the form of Eqn. (1) except insofar as to alter the magnitude of the axial dispersion coefficient due to increased gas mixing.

The last term on the right of Eqn. (1) corresponds to loss of tracer into the surrounding water phase. Thus, Eqn. (1) must be augmented by statements

about tracer uptake into the water sheaths and subsequently into the stagnant gas. These read in order:

$$\left[S_L/\left(S_T + S_F\right)\right] \frac{\partial C_L}{\partial t} + \frac{U_L}{U_{go}} \frac{\partial C_L}{\partial x} = Da \frac{\partial^2 C_L}{\partial y^2} \quad , \tag{3}$$

and

$$\alpha \frac{\partial C_T}{\partial t} = -Da \left. \frac{\partial C_L}{\partial y} \right|_{y=1} \quad , \tag{4}$$

where U_L is the average superficial velocity of the water sheaths.

Initial conditions are that of a core devoid of tracer: $C_i\ (0, x, y) = 0$ for i = T, F, and L. Boundary conditions are those of Danckwerts [20]:

$$C_F(t,0) - \frac{1}{Pe} \frac{\partial C_F(t,0)}{\partial x} = 1 \tag{5a}$$

and

$$\frac{\partial C_F(t,0)}{\partial x} = 0 \quad . \tag{5b}$$

Additionally, local equilibrium prevails at both extremities of the water sheath layers: $C_L\ (t, x, 0) = K\ C_F$ and $C_L\ (t, x, 1) = K\ C_T$. Here K is the tracer partition coefficient or Henry's constant defined as the equilibrium concentration of the tracer in the liquid divided by that in the gas (i.e., $K \equiv C_L/C_i$ for i = T, F). Ambient-temperature values of K for our CH_4 and SF_6 tracers are 0.033 and 0.0056, respectively [21].

Equations (1)-(5) supplemented by overall continuity of the gas phase are solved by the method of Laplace transforms with numerical inversion [21].

Fortunately, a number of useful simplifications arise. First, even for inlet to exit pressure ratios of up to 100 there is very little effect of gas compressibility. Accordingly, for the core lengths of our experiments, it is quite adequate to set P = 1. Second, our calculations indicate that both tracer convection and accumulation in the liquid sheaths are negligible. Hence, $S_L/(S_F + S_T)$ and U_L/U_{go} may confidently be set to zero in Eqn. (3). The physical justification is the very low liquid solubilities of the chosen tracer gases (i.e., $K < 10^{-2}$). In this case the mass transfer resistance of the intervening water cushions becomes passive in the sense that the tracer simply convectively diffuses across and into the stagnant gas. This second simplification is particularly important because knowledge of S_L and U_L is problematic. That is, not all of the liquid phase in the core physically separates flowing and trapped gas and constitutes the mass transfer resistant water sheaths.

With the two above approximations the mass transfer model appears similar to that of Coats and Smith [22], although the physical origin is quite distinct. Further, the parameters K and Da combine into a single product:

$$\beta = KDa = \phi\, S_L\, D_L\, LK/U_{go}\, \delta^2 \quad . \tag{6}$$

Now the ratio D_L/δ^2 takes on the meaning of a mass transfer coefficient multiplied by an effective interfacial area per unit volume. The remaining two model parameters are α and Pe.

Figure 3 reports calculated tracer histories for a trapped gas fraction of 85% and Pe = 1 as a function of the mass transfer parameter β. Local equilibrium with the trapped gas occurs for $\beta \geq 10$ while severe mass transfer limitations appear for $\beta \leq 1$. The early concentration rise followed by the later tailing with $\beta \leq 1$ typifies most of the available literature gas-tracer

experiments with foam [15-17]. The implication is that the previous tracer work was influenced by mass transfer limitations. More importantly, it means that gas-tracer experiments can be used to gauge trapped bubble saturations.

Also in the mass-transfer-limited regime, tracers with different values of β exhibit different tracer histories. This is the origin of the idea for using multiple tracers. In particular, if δ in Eqn. (6) is assumed to be independent of the specific tracer species, then β is proportional to the partition coefficient K and the liquid-phase diffusion coefficient D_L.

The ratio of β values for CH_4 to SF_6 is about 9 based on their known solubilities and diffusion coefficients in water [21]. In our fitting procedure to determine α, β, and Pe from the experimental methane and sulfur hexafluoride histories, we force α and Pe to be the same for each tracer gas while the values of β must be in the ratio of 9. Thus, two simultaneous histories are employed to obtain three parameters. We assert that this is a unique and powerful procedure which provides a vigorous test of both the experimental data and the proposed mass transfer model.

Another important feature of the histories for small β is the apparent asymptote at a dimensionless concentration of less than unity. This results from strongly delayed mass transfer into the stagnant gas. Eventually, for long times, all of the histories in Fig. 3 do asymptote to unity (i.e., the mean breakthrough time for all curves in Fig. 3 is unity). Thus, those histories that exhibit the fastest initial rise also exhibit the slowest approach to unity for long times. This observation is a valuable tool in the quantitative interpretation of the experimental gas-phase tracer histories.

EXPERIMENT

Apparatus

Figure 4 displays a schematic of the foam-flow apparatus. It is a modification of that of Ettinger and Radke [2] to allow for tracer injection and detection. Brine, 0.83 wt % NaCl (Mallinckrodt, reagent grade) in deionized and distilled water, with or without added surfactant, a 0.83 wt % active C_{14-16} α-olefin sulfonate (Bioterg AS-40, Stepan), is supplied by a high pressure piston pump (ISCO, Model 314). Flow of nitrogen (Liquid Air Corporation) and the tracer gas, a mixture of 15% methane, 15% sulfur hexafluoride, and 70% nitrogen by volume (Matheson Gas Products), is metered through mass flow controllers (Brooks, Model 5850) directly into the one.

The porous medium is a fired, Berea sandstone slab 20 cm (8 in) long x 10 cm (4 in) wide x 1.2 cm (0.4 in) deep with an absolute permeability of 2.3 μm^2 and a porosity of 0.24. Five differential transducers (Validyne, Model DP-15) monitor the pressure profile along the core, each relative to atmospheric pressure. Also, the differential pressure between the nitrogen and tracer gas delivery lines is measured downstream from the mass flow control valves to ensure matching pressures before introduction of the tracer mixture. A computer controlled and monitored scanning microwave attenuator detects the liquid saturation in the core [21,23,24].

Foam exiting the medium is readily broken in a phase splitter by a 10 wt % aqueous solution of Dow Corning Antifoam B. An in-house automatic, on-line sampling valve periodically sends gas to a chromatograph (Gow Mac, Model 550) for analysis. Excellent separation of the SF_6, N_2, and CH_4 is achieved on a molecular-sieve packed column (Varian 5A) with helium as the carrier gas. Output from the thermal conductivity detector is processed by an on-line data collection system controlled by a personal computer (IBM PCXT).

Back pressure is controlled at 10^5 Pa gauge (1 atm) with a simple, laboratory-constructed device consisting of a 2000-cm^3 vessel charged with regulated nitrogen pressure and vented through a precision needle valve. We find quite acceptable control to within approximately $\pm$ 50 Pa ($\pm$ 0.1 psi). Additional information on the apparatus design and operation is available in the thesis of Gillis [21].

Procedures

Steady foam flow was established in the oil-free core at a given nitrogen fractional flow (i.e., inlet foam quality) in the range from 0.8 to 1. Up to about 20 PV of total fluid was injected until the pressure profile and liquid saturation stabilized. Gas flow was then switched to the tracer mixture and exit concentrations were measured until they no longer increased. This new steady state required about 5 to 8 PV of fluid injection. Typical values of the relative detector concentrations were 8.8 for SF_6 and 4.5 for CH_4, with standard deviations of 0.1 and 0.2, respectively.

Afterwards, gas flow was switched back to untraced nitrogen, and new gas and liquid flows were set to another steady state. The tracer procedure was again repeated.

Effort was made to minimize dead volume in the system. Additionally, blank runs were made by replacing the core with a Temco (Model BPR-05) back pressure regulator whose dead volume is negligible. Tracer gas was injected and the system dead volume quantified. Core tracer histories were corrected accordingly.

Histories for Two-Phase Flow

As a check on the apparatus, several tracer experiments were performed for gas/brine flow with no surfactant present. A typical result is shown in

Fig. 5 where open ovals and solid squares represent the reduced exit concentrations of SF_6 and CH_4, respectively. A solid line gives the model fit for $\beta = 10^{-8}$ (i.e., an infinite resistance to tracer partitioning into the liquid phase). The simple mass transfer model shows excellent agreement with the experimental histories. The fit value for α, which in the case of no foam corresponds to the fraction of dentritic gas present, is 0.04. Thus, only 4% of the gas does not support flow. For the gas saturation of 40% pertinent to the two-phase flow in Fig. 5, we expect few dendrites (cf. Fig. 18 of [25]). Also, gas tracers are likely not very sensitive to dendrites because their diffusion coefficients, and hence mass transfer rates, are relatively large, compared to those of liquid tracers. Finally, we discover from the model fit that Pe = 1.16. For the interstitial gas velocity (i.e., $U_g/\phi\ S_g$) of 0.085 mm/s, the measured Peclet number specifies an axial dispersion coefficient of $D = 0.015\ cm^2/s$. This value compares quite favorably with those of Salter and Mohanty for dispersion coefficients of the nonwetting phase [25].

Figure 6 confirms the excellent reproducibility of our results for two sets of tracer histories during steady nitrogen/brine flow. Here, relative concentrations are graphed for ease of comparison. This is but one case of several studies made both with and without foam.

Histories for Foam Flow

Figure 7 displays sample SF_6 (ovals) and CH_4 (solid squares) concentration histories during steady foam flow for an injected quality of 0.89 and a total superficial velocity of 0.65 m/day. There is an early rise in tracer concentrations followed by a long tail to steady state compared to those in continuum biphasic flow (cf. Figs. 5 and 6). Note the measurable difference in the two tracer curves caused by the difference in brine solubility of these

two gases. The least soluble gas departs most from local equilibrium, as expected. These two curves strongly suggest the presence of trapped gas which exhibits significant mass transfer resistance to tracer partitioning.

Solid lines in Fig. 7 correspond to a best fit of the mass transfer model. Fitting is accomplished in time space by nonlinear least squares using a simplex scheme [26]. For the flow conditions imposed, about 75% of the gas is trapped (i.e., $\alpha = 0.76$). Thus, since the water saturation is close to 40%, only 15% of the pore space admits foam flow. Only the mass transfer parameter for SF_6 is reported (i.e., $\beta_{SF6} = 0.16$), since that for CH_4 is forced to be 9 times larger, as discussed earlier. When viewed in this manner, the fit of the methane history is quite sufficient.

Our fit values for the Peclet number are always very low, $Pe \lesssim 10^{-2}$. In the range of model parameters studied, tracer results are very sensitive to α and β but insensitive to Pe. Thus, changes in Pe of at least an order of magnitude do not materially alter the tracer histories. Nevertheless, the Peclet numbers we find are small. This seems to suggest significant axial mixing, possibly due to lamella making and breaking processes and/or highly branched flow paths at low flowing gas saturations.

RESULTS AND DISCUSSION

Table 1 lists some model-fit results for gas-bubble trapping in steady foam flow through Berea sandstone. Total flow velocities range from 0.44 to 4.1 m/day while fractional gas flows extend from 0.79 to 1.0. A unity fractional gas flow indicates only gas injection into the sandstone core containing connate surfactant solution (at a low water saturation near 0.2). Such experiments are not truly at steady state.

All of the experiments listed in Table 1 exhibit low flowing foam pressure drops. Typical foam flow resistance factors (i.e., FFR in [3]) are near 10. Such relatively small values are characteristic of weak foam flow [2,19] and presumably arise because of the low liquid and gas velocities studied in this work. That is, a critical pressure drop or velocity appears necessary to initiate a strong foam [2,17,19].

Numbers indicated in parentheses beside the α and β parameters reflect their uncertainty. Fitting to the proposed mass transfer model is precise for these two quantities. Thus, it appears that dual-gas tracer experiments, suitably interpreted, can extract quantitative measures of the stagnant gas.

The most important result from Table 1 is the large fraction of gas trapping, even in the case of no liquid flow. Values of almost 100% trapping are sometimes evident. We do not find a consistent trend of α with liquid or gas velocity. Possibly our studied range is not large enough. Such experiments need to be extended into the strong foam regime.

The mass transfer resistance parameter for sulfur hexafluoride, β in Table 1, has values near 0.1. Eqn. (6) and the assumption that all of the water in the porous medium parcels between the flowing and nonflowing foam (i.e., $S_L = S_w$) permit an estimate of the tracer resistant water layer thickness, δ. We find δ to be of order 300 μm. This is a reasonable physical value, since characteristic pore-body sizes for Berea sandstone are of order 100 μm [4,5]. This calculation lends further weight to the veracity of the mass transfer model.

CONCLUSIONS

The dual-gas tracer technique is a powerful new tool for assessing trapped gas saturation during steady foam flow through porous media. In this

technique, two tracer gases with differing liquid solubilities are injected in a step change. Quantitative trapped gas amounts are established by fitting the observed concentration histories to a macroscopic, convective-diffusion model.

A linear, lumped-parameter mass transfer model is proposed which pictures water sheaths of an average thickness separating the flowing and the blocked foam. This model is readily solved by Laplace transforms and well represents the experimentally observed tracer histories.

For weak foam flow in Berea sandstone over flow velocities from 1/2 to 4 m/day and over a quality range from 0.8 to 1.0, we find surprisingly large amounts of trapped gas. Usually the fraction of trapped gas is over 70%. In several cases, almost all of the gas is blocked. Such large fractions of trapped gas are an important ingredient to foam flow resistance and hence deserve further study.

NOMENCLATURE

c_{FL} = tracer concentration in effluent, kmol/m^3

$c_{FL}(\infty)$ = tracer concentration in effluent at infinite time, kmol/m^3

c_i = concentration of tracer in phase i, kmol/m^3

C_{FL} = $c_{FL}/c_{FL}(\infty)$, dimensionless concentration of tracer in the effluent

C_i = $c_i/c_{FL}(\infty)$, dimensionless tracer concentration in phase i

D = coefficient of axial dispersion, m^2/s

Da = $\phi\ S_L\ D_L\ L/U_{go}\ \delta^2$, Damköhler number

D_L = diffusion coefficient of the tracer in water intervening sheaths, m^2/s

f_g = $U_{go}/(U_{go} + U_w)$, inlet fractional flow of gas

K = equilibrium partition coefficient of tracer between water and gas

L = length of the core, m

P = P_g/P_{go}, dimensionless pressure

Pe = $U_{go}L/D$, Peclet number

P_g = gas pressure, Pa

S_i = saturation of phase i

t^* = time from the start of tracer injection, s

t = $t^*U_{go}/[\phi(S_F + S_T)L]$, dimensionless time

U_i = superficial velocity of phase i, m/s

U_{go} = superficial velocity of gas at core inlet, m/s

x^* = distance down the core, m

x = x^*/L, dimensionless axial distance

y^* = distance in the transverse direction, m

y = y^*/δ, dimensionless transverse distance

Greek

α = $S_T/(S_F + S_T)$, trapped gas fraction

β = K•Da, mass transfer resistance parameter

δ = characteristic thickness of the intervening, liquid-sheath phase, m

ϕ = porosity

Subscripts

F = flowing gas

g = gas

L = sheath liquid or effluent

T = trapped gas

w = total wetting liquid

o = inlet

ACKNOWLEDGEMENTS

This work was supported by the U.S. Department of Energy under Contract No. DC03-76SF00098 to the Lawrence Berkeley Laboratory of the University of California.

REFERENCES

1. Bernard, G.G. and Holm, L.W.: "Effect of Foam on Permeability of Porous Media to Gas," SPEJ (September 1964) 267-274.

2. Ettinger, R.A. and Radke, C.J.: "The Influence of Texture on Steady Foam Flow in Berea Sandstone," SPE 19688, presented at the 1989 Annual Fall Technical Conference of SPE, San Antonio, TX, October 8-11.

3. Persoff, P., Radke, C.J., Pruess, K., Benson, S.M. and Witherspoon, P.A.: "A Laboratory Investigation of Foam Flow in Sandstone at Elevated Pressure," SPE 18781, presented at the 1989 California Regional Meeting of SPE, Bakersfield, CA, April 5-7.

4. Chambers, K.T. and Radke, C.J.: "Capillary Phenomena in Foam Flow Through Porous Media," Interfacial Phenomena in Oil Recovery, Morrow, N.R., ed., Marcel Dekker, Chapter 6, to appear (1990).

5. Chambers, K.T.: "Pore-Level Basics for Modeling Foam Flow in Porous Media with Randomly Connected Pore Throats and Bodies," M.S. Thesis, University of California, Berkeley (1990).

6. Mast, R.F.: "Microscopic Behavior of Foam in Porous Media," SPE 3997, presented at the 1972 Annual Fall Technical Conference of SPE, San Antonio, TX, October 8-11.

7. Falls, A.H., Musters, J.J., and Ratulowski, J.: "The Apparent Viscosity of Foams in Homogeneous Beadpacks," SPERE (May 1989) 155-164.

8. Manlowe, D.J.: "Pore-Level Mechanisms of Foam Destabilzation by Oil in Porous Media," M.S. Thesis, University of California, Berkeley (1988).

9. Shirley, A.I.: "Foam Formation in Porous Media, A Microscopic Visual Study," Surfactant-Based Mobility Control, Smith, D.H. ed., ACS Symposium Series, Vol. 373, 234-257 (1988).

10. Prieditis, J.: "A Pore-Level Investigation of Foam Flow Behavior in Porous Media," Ph.D. Thesis, University of Houston (1988).

11. Rossen, W.R.: "Theories of Foam Mobilization Pressure Gradient," SPE/DOE 17358, presented at the 1988 SPE/DOE Enhanced Oil Recovery Symposium, Tulsa, OK, April 17-20.

12. Fried, A.N.: "The Foam-Drive Process for Increasing the Recovery of Oil," U.S. Dept. of Interior, Bureau of Mines (1961).

13. Persoff, P., Pruess, K., Benson, S.M., Wu, Y.S., Radke, C.J., Witherspoon, P.A. and Shikari, Y.A.: "Aqueous Foams for Control of Gas Migration and Water Coning in Aquifer Gas Storage," Energy Sources, to appear (1990).

14. Bernard, G.G., Holm, L.W., and Jacobs, W.L.: "Effect of Foam on Trapped Gas Saturation and on Permeability of Porous Media to Water," SPEJ (December 1965) 295-300.

15. Holm, L.W.: "The Mechanism of Gas and Liquid Flow Through Porous Media in the Presence of Foam," SPEJ (December 1968) 359-369.

16. Nahid, B.H.: "Non-Darcy Flow of Gas Through Porous Media in the Presence of Surface Active Agents," Ph.D. Thesis, University of Southern California, Los Angeles (1971).

17. Friedmann, F., Chen, W.H., and Gauglitz, P.A.: "Experimental and Simulation Study of High-Temperature Foam Displacement in Porous Media," SPE/DOE 17357, presented at the 1988 SPE/DOE Enhanced Oil Recovery Symposium, Tulsa, OK, April 17-20.

18. Jiménez, A.I. and Radke, C.J.: "Dynamic Stability of Foam Lamellae Flowing Through a Periodically Constricted Pore," Oil-Field Chemistry; Enhanced Recovery and Production Stimulation, Borchardt, J.K. and Yen, T.F., eds., ACS Symposium Series, Vol. 396, Chapter 25, 461-479 (1989).

19. Ransohoff, T.C. and Radke, C.J.: "Mechanisms of Foam Generation in Glass-Bead Packs," SPERE (May 1988) 573-585.

20. Danckwerts, P.V.: "Continuous Flow Systems: Distribution of Residence Times," Chem. Eng. Sci., Vol. 2 (1953) 1-13.

21. Gillis, J.V.: "Tracer-Detection and Structure of Stationary Lamellae During Foam Flow Through Berea Sandstone," Ph.D. Thesis, University of California, Berkeley (1990).

22. Coats, K.H. and Smith, B.D.: "Dead-End Pore Volume and Dispersion in Porous Media," SPEJ (March 1964) 73-84.

23. Sharma, D.K.: "Kinetics of Oil Bank Formation," Ph.D. Thesis, University of California, Berkeley (1987).

24. Ettinger, R.A.: "Flow Resistance of Foam in Berea Sandstone," M.S. Thesis, University of California, Berkeley (1989).

25. Salter, S.J. and Mohanty, K.K.: "Multiphase Flow in Porous Media: I. Macroscopic Observations and Modeling," SPE 11017, presented at the 1982 Annual Fall Technical Conference of SPE, New Orleans, LA, September 26-29.

26. Press, W.H., Flannery, B.P., Teukolsky, S.A. and Vetterling, W.T.: Numerical Recipes, Cambridge University Press, New York (1986).

Table 1. Trapped Gas Fraction During Steady Foam Flow Through a 2.3-μm^2 Berea Sandstone

U_g (m/day)	f_g	S_w	α	$^{\ddagger}\beta_{SF6}$
0.40	0.91	0.48	*0.75 ($\pm$ 0.005)	*0.13 ($\pm$ 0.008)
0.62	0.94	0.37	0.99 ($\pm$ 0.003)	0.19 ($\pm$ 0.002)
1.23	0.97	0.35	0.99 ($\pm$ 0.003)	0.13 ($\pm$ 0.001)
2.32	0.98	0.36	0.98 ($\pm$ 0.06)	0.02 ($\pm$ 0.01)
2.72	0.99	0.36	0.94 ($\pm$ 0.005)	0.11 ($\pm$ 0.005)
0.59	0.79	0.66	0.81 ($\pm$ 0.017)	0.19 ($\pm$ 0.02)
0.57	0.89	0.38	0.76 ($\pm$ 0.006)	0.16 ($\pm$ 0.01)
0.70	0.99	0.39	0.76 ($\pm$ 0.01)	0.34 ($\pm$ 0.01)
$^{+}$0.73	1.00	0.21	0.72 ($\pm$ 0.003)	0.16 ($\pm$ 0.006)
$^{+}$0.73	1.00	0.21	0.72 ($\pm$ 0.003)	0.16 ($\pm$ 0.006)
2.60	1.00	0.21	0.79 ($\pm$ 0.008)	0.15 ($\pm$ 0.01)
4.08	1.00	0.20	0.86 ($\pm$ 0.005)	0.10 ($\pm$ 0.008)

$^{+}$These values are from the same experiment.

*Numbers in parentheses give estimates of the standard deviation of the fit parameter value.

‡The values of β for CH_4 are 9 times larger.

FIGURE CAPTIONS

Figure 1. Trapping of foam clusters at small, liquid-filled pore throats and at small, diverging pore throats. Trapped foam is indicated by shading while flowing foam appears clear. Arrows highlight the two pore throats responsible for trapping.

Figure 2. Pore-level schematic of foam microstructure in porous media. Cross hatched space indicates solid grains (shown uncemented) and dotted space reflects wetting liquid. Foam bubbles are clear (flowing) and shaded (trapped). Larger pore channels are located sequentially towards the top of the picture.

Figure 3. Tracer histories calculated from the mass transfer model for Pe = 1 and 85% trapped gas (i.e., $\alpha = 0.85$). Small values of β show large deviations from local equilibrium.

Figure 4. Schematic of the experimental apparatus.

Figure 5. Experimental tracer histories for steady nitrogen/brine flow. The solid line is a fit of the mass transfer model with no partitioning into the liquid phase (i.e., $\beta \sim 0$).

Figure 6. Reproducibility of experimental tracer histories for two nitrogen/brine flows.

Figure 7. Experimental tracer histories for steady foam flow. In this case 76% of the gas is trapped (i.e., $\alpha = 0.76$).

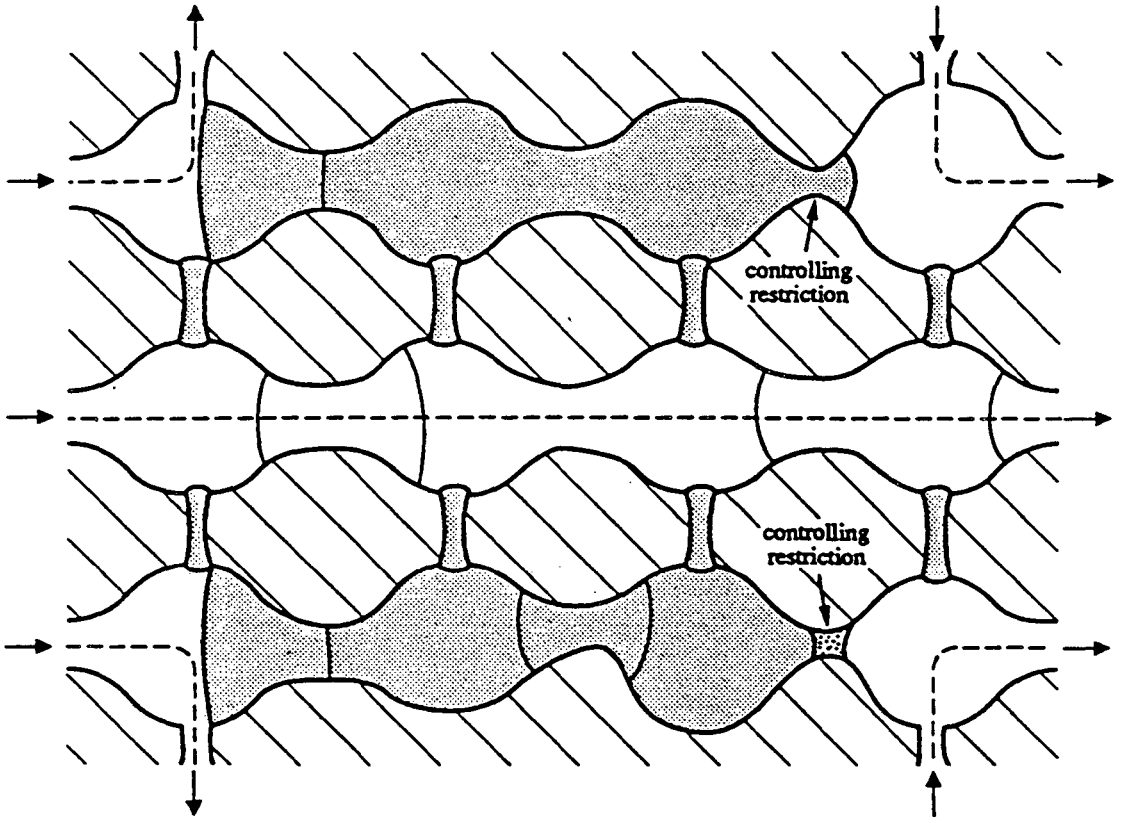

Figure 1

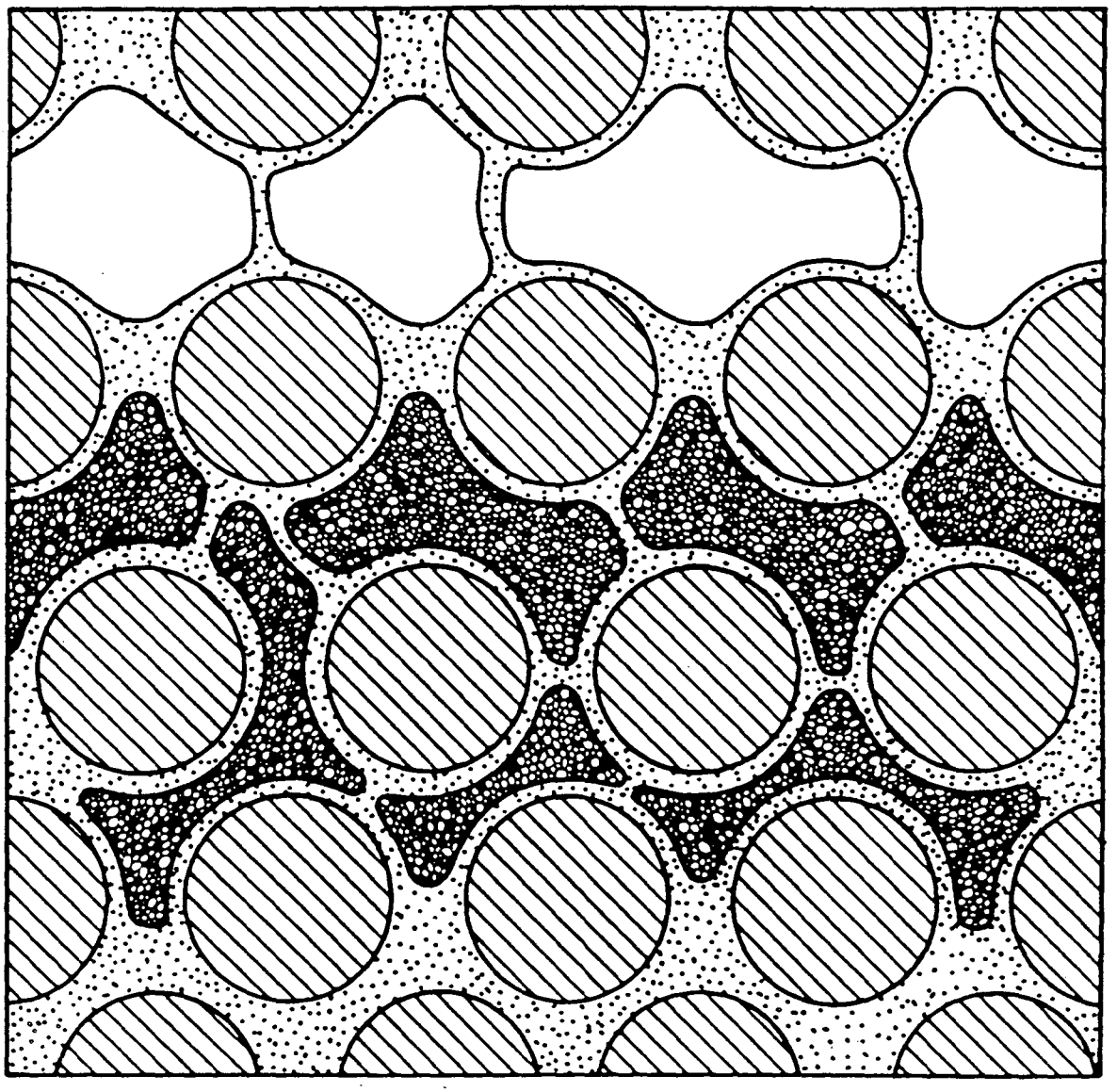

Figure 2

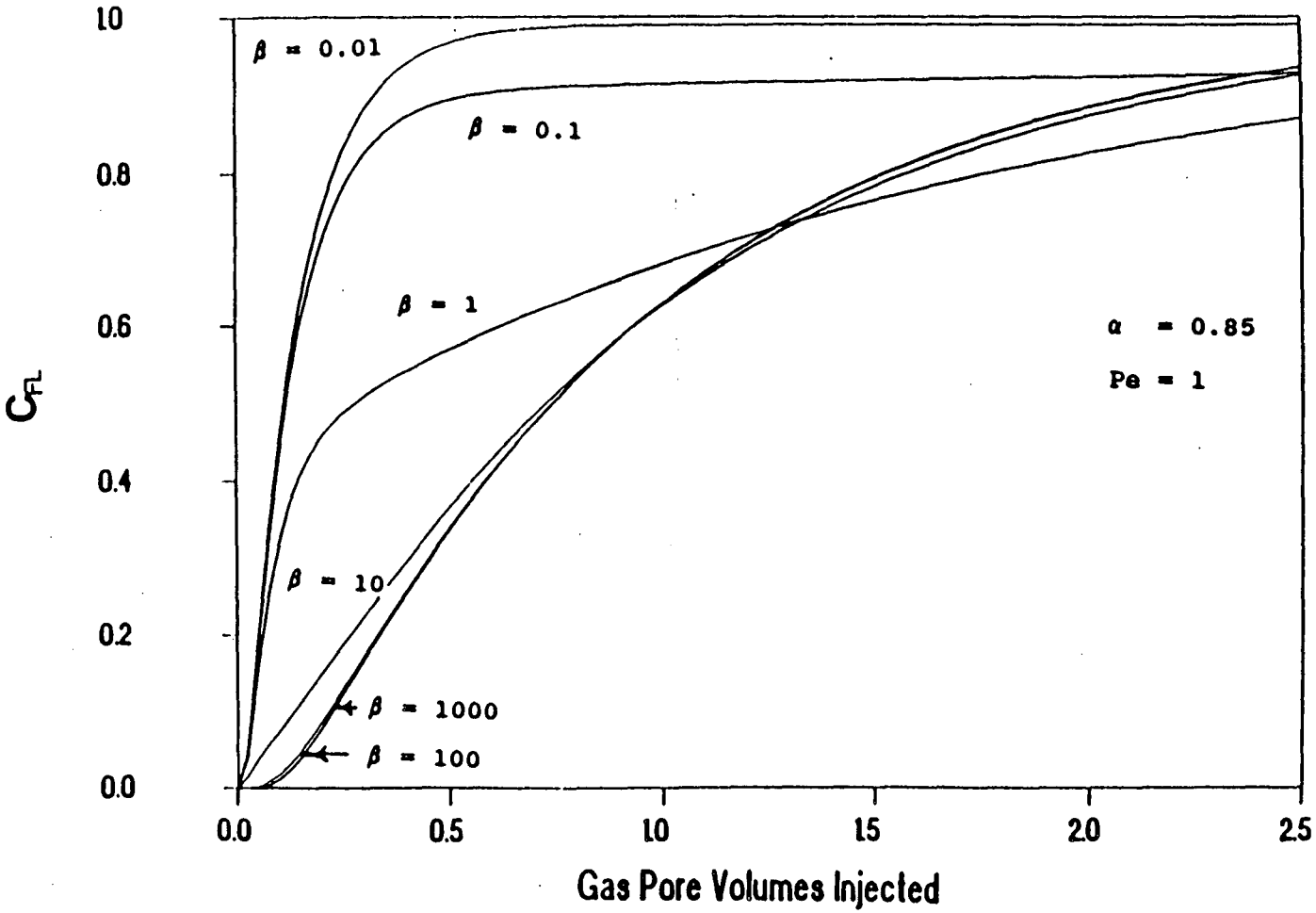
1.0
0.8
0.6
0.4
0.2
0.0
C_{FL}
β = 0.01
β = 0.1
β = 1
β = 10
β = 1000
β = 100
α = 0.85
Pe = 1
0.0
0.5
1.0
1.5
2.0
2.5
Gas Pore Volumes Injected

Figure 3

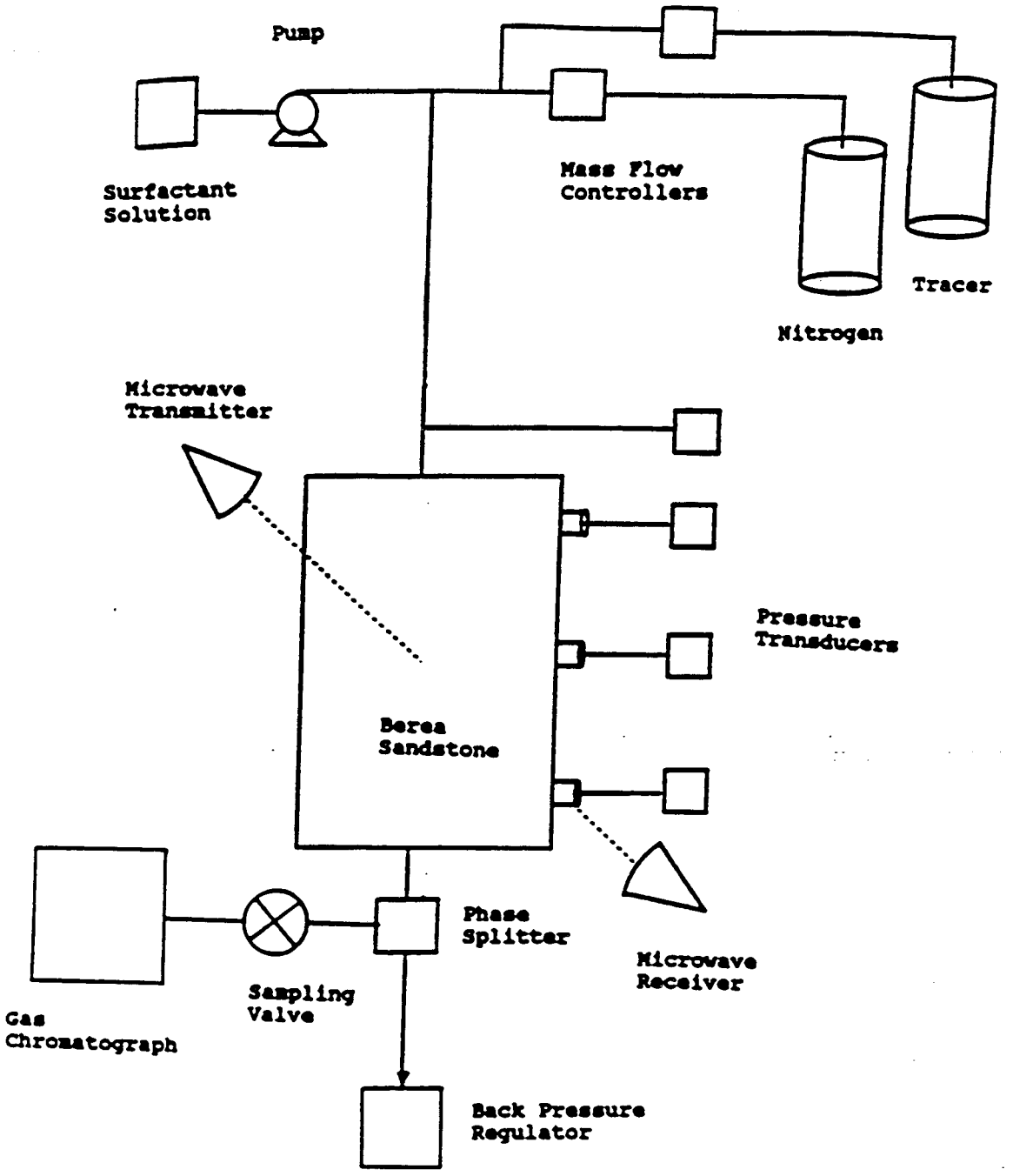
Pump
Surfactant Solution
Mass Flow Controllers
Tracer
Nitrogen
Microwave Transmitter
Pressure Transducers
Berea Sandstone
Phase Splitter
Microwave Receiver
Sampling Valve
Gas Chromatograph
Back Pressure Regulator

Figure 4

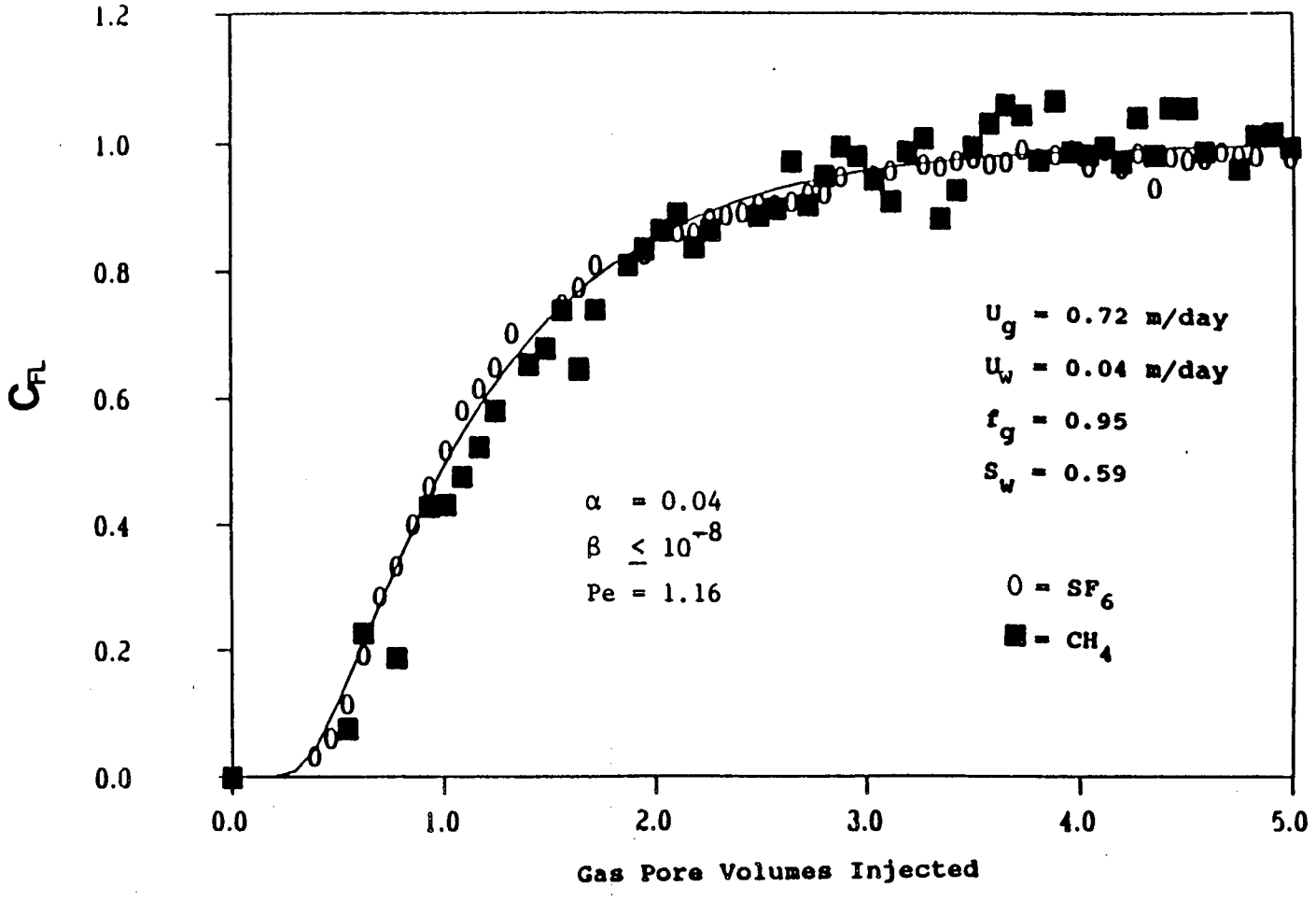
1.2
1.0
0.8
0.6
0.4
0.2
0.0
C_{FL}
0.0
1.0
2.0
3.0
4.0
5.0
Gas Pore Volumes Injected
U_g = 0.72 m/day
U_w = 0.04 m/day
f_g = 0.95
S_w = 0.59
α = 0.04
β ≤ 10^{-8}
Pe = 1.16
0 = SF_6
■ = CH_4

Figure 5

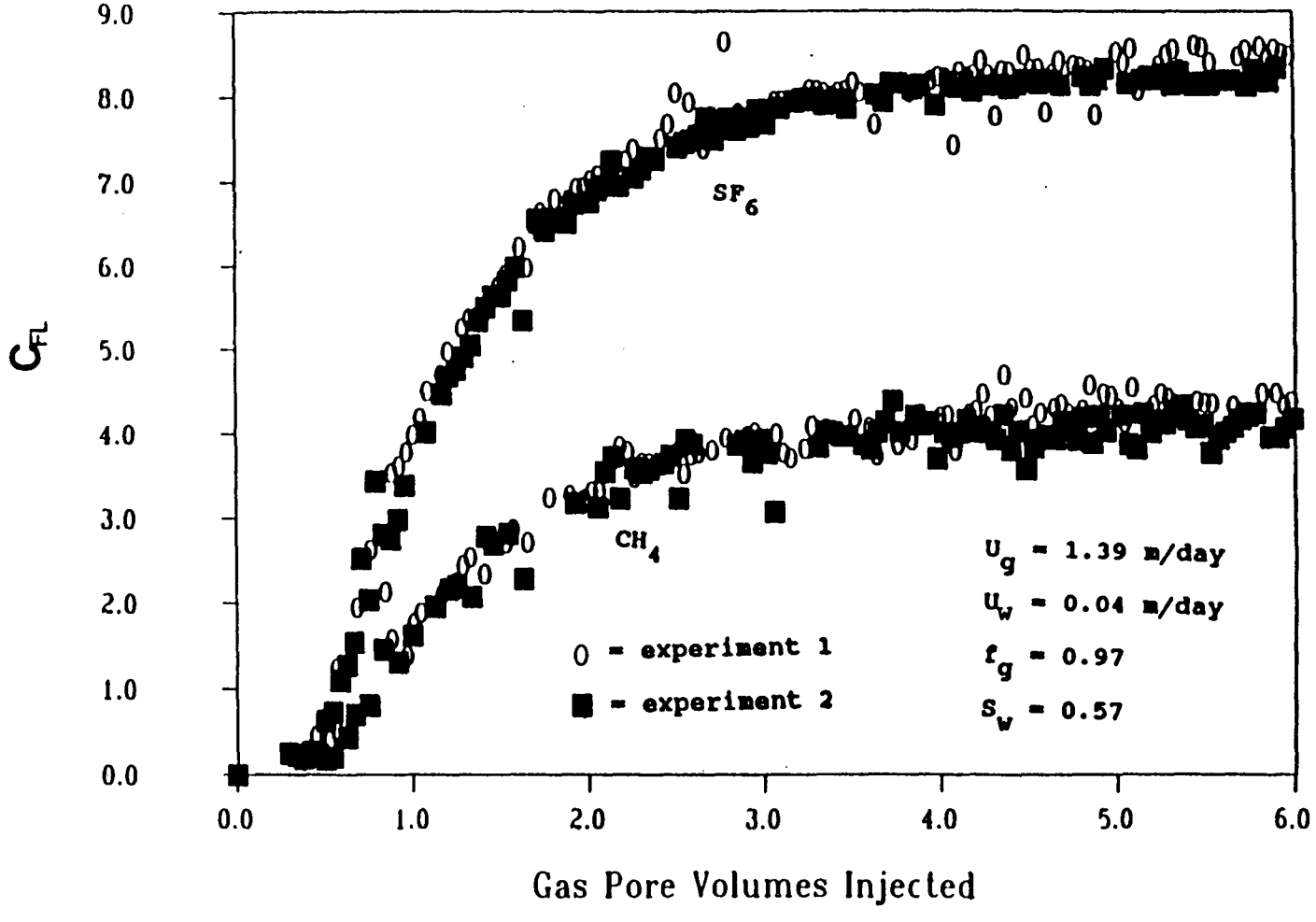
9.0
8.0
7.0
6.0
5.0
4.0
3.0
2.0
1.0
0.0
C_{FL}
0.0
1.0
2.0
3.0
4.0
5.0
6.0
Gas Pore Volumes Injected
SF_6
CH_4
0 = experiment 1
■ = experiment 2
U_g = 1.39 m/day
U_w = 0.04 m/day
f_g = 0.97
S_w = 0.57

Figure 6

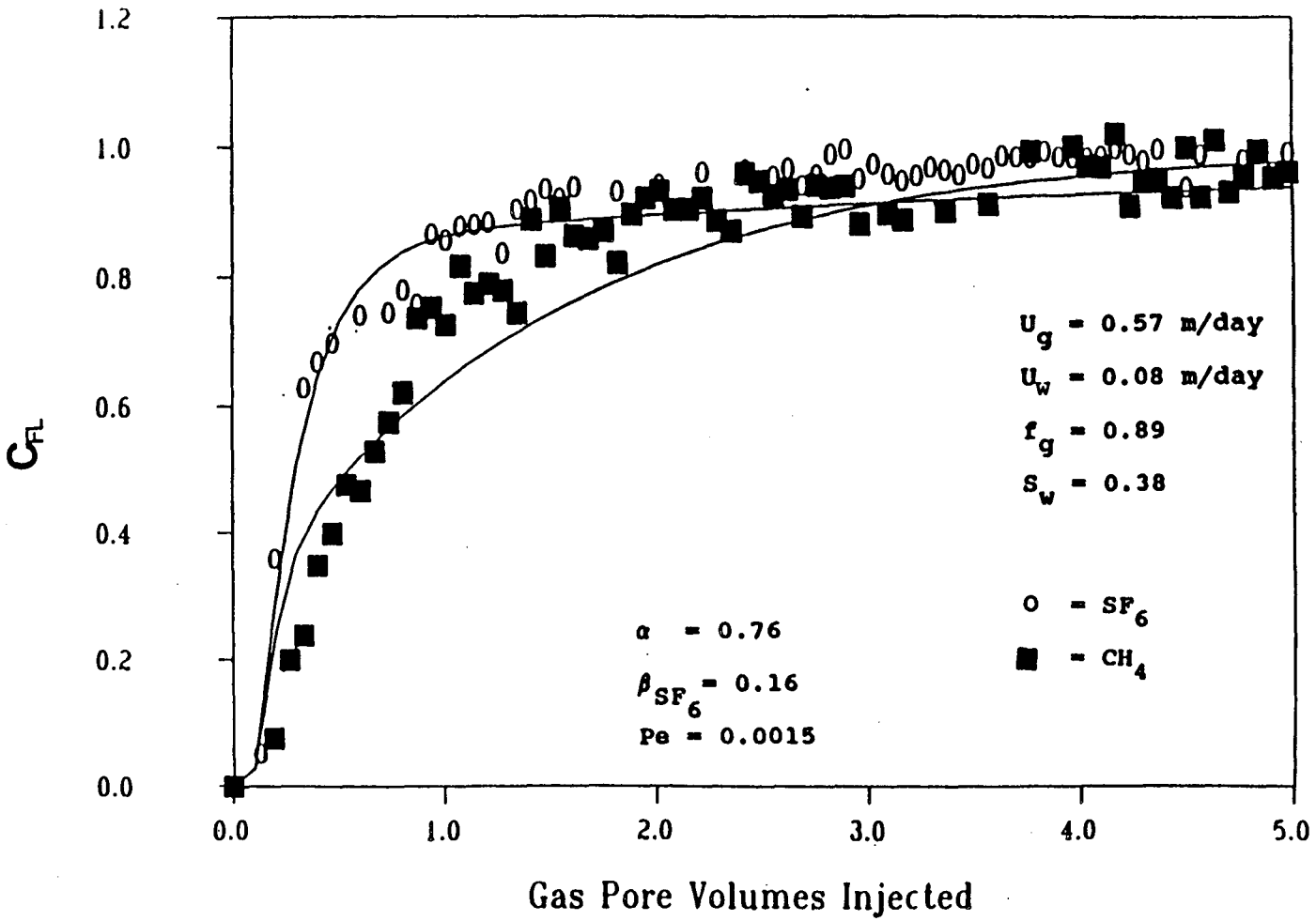
1.2
1.0
0.8
0.6
0.4
0.2
0.0
C_{FL}
0.0
1.0
2.0
3.0
4.0
5.0
Gas Pore Volumes Injected
U_g = 0.57 m/day
U_w = 0.08 m/day
f_g = 0.89
S_w = 0.38
O = SF_6
■ = CH_4
α = 0.76
β_{SF_6} = 0.16
Pe = 0.0015

Figure 7

LAWRENCE BERKELEY LABORATORY
UNIVERSITY OF CALIFORNIA
INFORMATION RESOURCES DEPARTMENT
BERKELEY, CALIFORNIA 94720